State of Environment Report 2001 - 2006/7

Chief Editor, Prof. Dr. Temel Oguz, Institute of Marine Sciences, Middle East Technical University, Erdemli, Turkey

Chapter 1A - General Oceanographic Properties: Physico-chemical and Climatic Featuers

CHAPTER 1A. GENERAL OCEANOGRAPHIC PROPERTIES: PHYSICO-CHEMICAL AND CLIMATIC FEATURES

Temel Oguz

Institute of Marine Sciences,

Middle East Technical University, Erdemli, Turkey

1A.1. Main physical and chemical features

The Black Sea is a strongly stratified system; its stratification within the upper 100 m layer (10% of the entire water column) varies up to a density of s_t ~5 kg m^{-3} (Fig. 1A.2.1) and is an order of magnitude greater than, for example, in the neighboring Mediterranean Sea. The pycnocline corresponding to the density surface s_t ~16.2 kg m^{-3} approximately conforms to 150 m depth within the interior cyclonic cell or may extend to 200 m within coastal anticyclones. The deep homogenous layer that has a thickness of 2000 m within the abyssal plain of the sea possesses almost vertically uniform characteristics below 200 m within the range of values of temperature (T) of ~ 8.9-9.1ºC, salinity (S) of ~ 22-22.5, and s_t ~ 17.0-17.3 kg m^{-3}. The deepest part of the water column approximately below 1700 m involves homogeneous water mass formed by convective mixing due to the bottom geothermal heat flux during the last several thousands of years (Murray et al., 1991).

Fig. 1A.2.1. Vertical variations of temperature (ºC) and density (expressed in terms of sigma-t, kg m^{-3}) at various locations of the interior basin during different months representing different types of vertical structures (the data are retrieved from the IMS-METU data base; http: sfp1.www.ims.metu.tr/ODBMSDB/).

The upper 50-60 m is homogenized in winter with T~6-7 ºC, S ~18.5-18.8, s_t ~14.0-14.5 kg m^{-3} when the northwestern shelf and near-surface levels of the deep basin exposed to strong cooling by successive cold-air outbreaks, intensified wind mixing, and evaporative loss. Two examples are depicted in Fig. 1A.2.1 for the interior cyclonic cell at the time of intermediate level convection event during 14 February, 1990 and immediately after one of the most severe winters of the last century (April 3, 1993) during which the mixed layer temperature reduced to ~5.5 ºC. Yet another observation of winter convection event within an anticyclonic eddy closer to the southern coast (41.39ºN, 30ºE) during March 2003 is shown in Fig. 1A.2.1. This event cooled the surface mixed layer to 6.5?C within 90 m layer that is roughly twice deeper than those observed in the cyclonic interior basin.

As the spring warming stratifies the surface water, the remnant of the convectively-generated cold layer is confined below the seasonal thermocline and forms the Cold Intermediate Layer (CIL) of the upper layer thermohaline structure (Fig. 1A.2.1). Following severe winters, the CIL may preserve its structure for the rest of the year, but it may gradually warm up and loose its character in the case of warm winter years. These alternative structures are shown in Fig. 1A.2.1. Stratification in summer months comprises a surface mixed layer with a thickness of 10-20 m with T~22-26ºC, S~18-18.5 and s_t ~10.5-11.5 kg m^{-3}.

An important feature of the upper layer physical structure is the intensity of diapycnal mixing that controls ventilation of the CIL and oxygen deficient zone and nutrient entrainment from its subsurface source in winter months. According to the recent microstructure measurements (Gregg and Yakushev, 2005 and Zatsepin et al. 2007), the vertical diffusivity attains its maximal values on the order of 10^{-3}? 10^{-4} m^2 s^{-1} in the surface mixed layer (0?15 m), but decreases to? 10^{-5}?10^{-6} m^2 s^{-1} across the seasonal thermocline (15?30 m). An increase in the diapycnal diffusivity is observed in the CIL to the range 2?6 x 10^{-5} m^2 s^{-1}. Below the base of the CIL, it rapidly decreases to its background values of 1?4?10^{-6} m^2 s^{-1}. Consequently, turbulent fluxes near the base of CIL are too weak to renew the oxygen deficient Suboxic Layer (SOL).

The Mediterranean underflow that is characterized typically by T~13-14 ºC and S~35-36 upon issuing from the Bosporus modifies considerably by mixing with the upper layer waters and enters the shelf with T~12-13 ºC and S~28-30. In the shelf, its track is regulated by small scale topographic variations. As it spreads out as a thin layer along the bottom, it is diluted by entrainment of relatively colder and less saline CIL waters and is barely distinguished by its slight temperature and salinity differences from the ambient shelf waters up on issuing the shelf break. The modified Mediterranean water is then injected in the form of thin multiple layers at intermediate depths (150-250 m) (Hiscoock & Millero, 2006; Glazer et al, 2006). Signature of the Mediterranean inflow within the interior parts of the basin can be best monitored up to 500 m, where the residence time of the sinking plume varies from ~10 years at 100 m depth to ~400 years at 500 m (Ivanov and Samodurov, 2001; Lee et al., 2002).

The upper layer biogeochemical structure that overlies the deep and lifeless anoxic pool (except anaerobic bacteria) involves four distinct layers (Fig. 1A.2.2). The uppermost part extending to the depth of 1% light level (a maximum thickness of nearly 50 m) characterizes active biological processes (e.g. nutrient uptake, plankton grazing, mortality, microbial loop, etc.), high oxygen concentrations (~300 ?M) and seasonally varying nutrient and organic material concentrations supplied laterally from rivers and coastal zones and vertically from sub-surface levels through vertical mixing. In the interior basin, surface mixed layer waters are poor in nutrients for most of the year except occasional incursions from coastal regions and by wet precipitation. Below the seasonal thermocline and in the deeper part of the euphotic zone, nutrient concentrations increase due to their recycling as well as continuous supply from the nutricline. Nitrate accumulation in this light-shaded zone generally supports summer subsurface phytoplankton production. In winter, nutrient stocks in the euphotic zone are renewed from the nutricline depths through upwelling, vertical diffusion and seasonal wind and buoyancy-induced entrainment processes and depleted by biological utilization.

Fig. 1A.2.2. O_2 and H_2S profiles (left) and NO_3, NO_2 and NH_4 profiles (right) versus density expressed in sigma-t (kg m^{-3}) in the center of the eastern gyre of the Black Sea during May 2003. The data source: http://www.ocean.washington.edu/cruises/Knorr2003/index.html.

The euphotic layer oxygen concentration undergoes pronounced seasonal variations within a broad range of values from about 250 to 450 ?M. The period from the beginning of January until mid-March exhibits vertically uniform mixed layer concentrations of ~300-350 ?M, ventilating the upper ~50 m of the water column as a result of convective overturning. The rate of atmospheric oxygen input in the ventilation process is proportional to the excess of saturated oxygen concentration over the surface oxygen concentration. The maximum contribution of oxygen saturation is realized towards the end of February during the period of coolest mixed layer temperatures, coinciding with the maximum and deepest winter oxygen concentrations during the year. After March, initiation of the warming season is accompanied by oxygen loss to the atmosphere and decreasing solubility, thus reducing oxygen concentrations within the uppermost 10 m to 250 ?M during the spring and summer months. A subsequent linear trend of increase across the seasonal thermocline links low near-surface oxygen concentrations to relatively higher sub-thermocline concentrations. Depending on the strength of summer phytoplankton productivity, the sub-thermocline concentrations exceed 350 ?M in summer.

The upper boundary of oxycline where oxygen concentration starts decreasing from ~300 µM corresponds to s_t ~14.4?14.5 kg m^{-3} (35?40 m) isopycnal surfaces in cyclonic regions (Fig. 1A.2.2) and s_t ~14.0?14.2 kg m^{-3} (70?100 m) in coastal anticyclonic regions (Fig. 1A.2.3). The lower boundary of oxycline is defined by 10 µM oxygen concentration located generally at s_t ~15.6 kg m^{-3}. Oxygen concentrations finally vanish above the anoxic interface located at s_t ~16.2 kg m^{-3}. The oxygen deficient (O_2 < 10 ?M), non-sulfidic layer having a thickness of 20-to-40 m coinciding with the lower nitracline zone is referred to as the "Suboxic Layer (SOL)" (Fig. 1A.2.2). Since identified by Murray et al. (1989, 1991), it has been observed consistently all over the basin with almost similar characteristics. Analyzing the available data after the 1960s, Tugrul et al. (1992), Buesseler et al. (1994) and Konovalov and Murray (2001) showed that the suboxic zone was present earlier, but it was masked in the observations because of low sampling resolution and contamination of water samples with atmospheric oxygen. These earlier observations measured dissolved oxygen concentrations more than 10 ?M inside the sulfidic layer (Sorokin, 1972; Faschuk, et al., 1990; Rozanov et al., 1998).

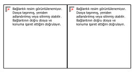

Fig. 1A.2.3. Vertical distribution of temperature (T), salinity (S), transmission (Trans), oxygen (O_2), hydrogen sulfide (H_2S), total manganese (Mn_2^+), silicates (Si), nitrates (NO_3), nitrites (NO_2), ammonia (NH_4), urea (Urea), phosphates (PO_4), and organic phosphorus (Porg) at a summer station near Gelendzhik, along the eastern coast of the Black Sea. Concentrations of chemical parameters are in µM (after Yakushev et al., 2005).

The SOL structure is subject to temporal and regional modifications during the periods of enhanced phytoplankton production in the surface layer. For example, the R.V Knorr May-June 2001 survey conducted within the western basin during a phytoplankton bloom episode (Oguz and Ediger, 2007) showed gradual change in the position of the oxycline and the upper boundary of the SOL up to σ_t~15.15 kg m^{-3} within less than a month.? On the other hand, the oxygen profiles in the southwestern Black Sea shelf-slope region displayed another extreme case with lenses of high oxygen content (~20 µM) within the Suboxic Layer and its interface with the anoxic layer due to the intrusions of relatively oxygen rich Mediterranean underflow (Hiscoock & Millero, 2006; Glazer et al, 2006). In anticyclones, the upper boundary of SOL is located at deeper levels (~15.8 kg m^{-3}) and therefore the SOL is relatively shallow (around 10-20 m) (Oguz et al., 2003).

Only a small fraction (~10%) of particulate flux is exported to deeper anoxic part of the sea (Lebedeva and Vostokov, 1984; Karl and Knauer, 1991). This loss is compensated excessively by lateral nitrogen supply mainly from the River Danube, by wet deposition and nitrogen fixation. The nutrient fluxes of anthropogenic origin are transported across the shelf and around the basin through the Rim Current system, and spread ultimately over the interior basin and form a major source of nitrate enrichment of the euphotic zone, while some is lost through Bosporus surface flow (Polat and Tugrul, 1995). The river influence markedly weakens toward the south along the coast and offshore for most of the year due to photosynthetic consumption of dissolved inorganic nutrients and sedimentation within the northwestern and western shelves. The river supply gives rise to a high N/P ratio within northwestern-western shelf that makes phosphate as the primary limiting nutrient along the coastal zone. The outer shelf appears to possess weakly nitrogen or phosphorus limited system, but the interior basin and major part of the sea is strongly nitrogen limited.

When nitrate profiles are plotted against density, the position of its peak concentration (6.0 ? 2.0 ?M) coincides approximately with the s_t ~15.5 ? 0.1 kg m^{-3} level (Figs. 1.2.2

and 1.2.3). Some degree of variability is, however, observed in its position and concentration in the western interior basin particularly in the vicinity of the wide topographic slope zone adjacent to the northwestern shelf. The nitrate structure is accompanied by occasional peaks of ammonium and nitrite on the order of 0.5 ?M and 0.1 ?M, respectively, near the base of the euphotic zone due to inputs from excretion and aerobic organic matter decomposition following subsurface plankton production (Fig. 1A.2.2). They, however, rapidly deplete below the euphotic zone.?

Within the oxygen deficient layer below s_t ~15.6 kg m^{-3}, organic matter decomposition via denitrification, and oxidation of reduced manganese and iron result in a sharp decrease of nitrate concentration to trace values at s_t ~16.0 kg m^{-3} isopycnal surface (Figs. 1.2.2 and 1.2.3). As nitrate is reduced to nitrogen gas, nitrite formed as an intermediate product marks the limits of denitrification zone; its peak concentration up to 0.2 ?M is usually observed at s_t ~15.85?0.05 kg m^{-3} (Fig. 1A.2.2 and 1.2.3). Nitrite is often used to oxidize ammonium (the anammox reaction; $NO_2^- + NH_4^+ \rightarrow N_2$) as documented recently (Kuypers et al., 2003). The deep sulphide-bearing waters contain no measurable nitrate, but constitute large pools of ammonium and dissolved organic nitrogen. Ammonium concentration increases sharply below s_t ~16.0 kg m^{-3}, reach at values of 10 ?M at 150 m (s_t ~16.5 kg m^{-3}) and 20 ?M at 200 m (s_t ~16.8 kg m^{-3}) (Fig. 1A.2.3). The gradient of ammonium profiles in the vicinity of the suboxic-anoxic interface suggests no ammonium supply to the euphotic zone from the anoxic region.

The vertical structure of phosphate concentration resembles nitrate in the upper layer but has a more complex structure in the suboxic-anoxic layers (Fig. 1A.2.3). Phosphate concentrations increase gradually within the deeper part of euphotic layer up to a maximum value of 1.0-1.5 ?M around s_t ~15.6 kg m^{-3}, and then decreases to minimum of about 0.5 ?M at s_t ~15.9?0.1 kg m^{-3} where nitrite locally displays a peak. It then increases abruptly to peak values of 5.0-8.0 ?M near s_t ~16.2 kg m^{-3} that coincides with the first appearance of sulfide in the water column and therefore coincides with the anoxic boundary. Formation of this peak has been explained by dissolution of phosphate-associated iron and manganese oxides. Silicate possesses a relatively simple vertical structure with a steady increase of concentrations below the euphotic layer up to about 70-75 ?M at s_t ~16.2 kg m^{-3} and then to about 150 ?M at s_t ~16.8 kg m^{-3} (Fig. 1A.2.3).

The boundary between the suboxic and anoxic layers involves a series of complicated redox processes. As dissolved oxygen and nitrate concentrations vanish, dissolved manganese, ammonium and hydrogen sulfide concentrations begin to increase (Fig. 1A.2.3). Marked gradients of particulate manganese around this transition zone near s_t ~16.0 kg m^{-3} reflect the role of manganese cycling. The deep ammonium, sulfide and manganese pools have been accumulating during the last 5000 years as a result of organic matter decomposition after the Black Sea has been converted into a two-layer stratified system.

The anaerobic sulfide oxidation and nitrogen transformations coupled to the manganese and iron cycles form the first-order dynamics maintaining stability of the interface structure between the suboxic and anoxic layers. The upward fluxes of sulfide and ammonium are oxidized by Mn(III, IV) and Fe(III) species, generated by Mn(II) and Fe(II) oxidation in reactions with nitrate. The upward flux of ammonium is also oxidized by NO_2^- via anammox reaction (Kuypers et al., 2003). These oxidation-reduction reactions are microbially catalyzed, but dissolved chemical reduction may also play a role in Mn(IV) reduction with sulfide. Trouwborst et al. (2006) have recently shown the key role of soluble Mn(III) in manganese catalytic redox cycle. Mn(III) acquires a second peak at the top of the SOL, just below the layer where O_2 disappears and particulate and dissolved manganese starts increasing with depth.

Anaerobic photosynthesis is an additional mechanism contributing to the oxidation-reduction dynamics near the anoxic interface. The reduced chemical species (HS^-, Mn^{2+}, Fe^{2+}) are oxidized by anaerobic phototrophic bacteria in association with phototrophic reduction of CO_2 to form organic matter. This mechanism was supported by the discovery of large quantities of bacteriochlorophyll pigments near the suboxic-anoxic boundary (Repeta et al., 1989; Repeta and Simpson, 1991; Jorgensen et al., 1991; Jannasch et al., 1991). A particular bacterium is capable of growth using reduced S (H_2S or S^0) at very low light levels (<<0.1% of the incident radiation at the surface). Its contribution, however, is mostly limited to cyclonic regions where the anoxic interface zone is shallow enough to be able to receive sufficient light to maintain photosynthetic activity. The third mechanism is direct oxidation of H_2S by oxygen and particulate manganese near the interface layer. Konovalov and Murray (2001) show that more than 50% of the upward flux sulfide could be consumed by this pathway.

1.2.2. Circulation characteristics

The upper layer waters of the Black Sea are characterized by a predominantly cyclonic, strongly time-dependent and spatially-structured basin-wide circulation. Many details of the circulation system have been explored by the recent hydrographic data (Oguz et al., 1994; 1998; Oguz and Besiktepe, 1999; Gawarkiewicz et al., 1999; Krivosheya et al., 2000), Lagrangian floats (Afanasyev et al., 2002; Poulain et al., 2005; Oguz et al., 2006), the satellite AVHRR and ocean color data (Oguz et al., 1992; Sur et al., 1994, 1996; Sur and Ilyin, 1997; Ozsoy and Unluata, 1997; Ginsburg et al., 2000, 2002a,b; Afanasyev et al., 2002; Oguz et al., 2002a; Zatsepin et al., 2003), altimeter data (Korotaev et al., 2001 and 2003; Sokolova et al., 2001), as well as modeling studies (e.g. Oguz et al.,1995; Stanev and Beckers, 1999; Besiktepe et al., 2001; Staneva et al., 2001; Beckers et al., 2002; Korotaev et al., 2003).

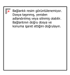

Fig. 1A.2.4. A typical structure of the upper layer circulation field deduced from a circulation model using assimilation of altimeter sea level anomaly data as described by Korotaev et al. (2003).?

These analyses reveal a complex, eddy-dominated circulation with different types of structural organizations of water masses within the interior cyclonic cell, the Rim Current jet confined mainly along the abruptly varying continental slope and margin topography around the basin, and a series of anticyclonic eddies along onshore side of the Rim Current (Fig. 1A.2.4). The interior circulation consists of several sub-basin scale gyres, each of which is formed by several cyclonic eddies. They evolve continuously by interactions among each other, as well as with meanders and filaments of the Rim Current. The overall basin circulation is primarily forced by the curl of wind stress throughout the year, and further modulated by the seasonal evolution of the surface thermohaline fluxes and mesoscale features arising from the basin?s internal dynamics. The strong topographic slope together with the coastline configuration of the basin governs the main pattern of the Rim Current system but it modulates seasonally from a more coherent structure in the winter and spring to more turbulent structure in the late summer and autumn. The fresh water discharge from the Danube contributes to buoyancy-driven component of the basin-wide cyclonic circulation system. Baroclinic instability processes are responsible by introducing considerable variability of the Rim Current in the form of eddies, meanders, filaments, offshore jets that propagate cyclonically around the basin. Over the annual time scale, westward propagating Rossby waves further contribute to the complexity of basin wide circulation system (Stanev and Rachev, 1999). Eddy dynamics and mesoscale features evolving along the periphery of the basin as part of the Rim Current dynamic structure appear to be the major factor for the shelf-deep basin exchanges. They link coastal biogeochemical processes to those beyond the continental margin, and thus provide a mechanism for two-way transports between near shore and offshore regions.

The ship mounted Acoustic Doppler Current Profiler (ADCP) and CTD measurements in the western Black Sea (Oguz and Besiktepe, 1999), carried out soon after an exceptionally severe winter conditions in 1993, provided striking findings in regards to the intensity and vertical structure of Rim Current in the western basin. The data has shown a vertically uniform current structure in excess of 50 cm/s (maximum value ~100 cm/s) within the upper 100 m layer, followed by a relatively sharp change across the pycnocline (between 100 and 200 m) and the vertically uniform sub-pycnocline currents of 20 cm/s (maximum value ~40 cm/s) up to 350 m being the approximate limit of ADCP measurements. The cross-stream velocity structure exhibited a narrow core region (~30 km) of the Rim Current jet that was flanked by a narrow zone of anticyclonic shear on its coastal side and a broader region of cyclonic shear on its offshore side. Such exceptionally strong sub-pycnocline currents of the order of 20-40 cm/s should be largely related with the severity of the winter conditions that was indeed one of the most severe winters of the last century (Oguz et al., 2006). The corresponding geostrophically-estimated currents from the CTD measurements were relatively weak due to the lack of ageostrophic effects and barotropic component of the current.

Contrary to the jet-like flow structure over the continental slope along the southern coast, the currents measured by ADCP over the northwestern shelf (NWS) were generally weaker than 10 cm/s (Oguz and Besiktepe, 1999). Relative weakness of the shelf currents is consistent with the fact that the continental slope acts as an insulator limiting the effects of Rim Current and mesoscale features propagating over the wide topographic slope zone between the NWS and the deep interior.

Apart from complex eddy-dominated features, larger scale characteristics of the upper layer circulation system possess a distinct seasonal cycle (Korotaev et al., 2003; Poulain et al., 2005). The interior cyclonic cell in winter months involves a well-defined two-gyre system surrounded by a rather strong and narrow jet without much lateral variations. This system gradually transforms into a multi-centered composite cyclonic cell surrounded by a broader and weaker Rim Current zone in summer. The interior flow field finally disintegrates into smaller scale cyclonic features in autumn (September-November) in which a composite Rim Current system is hardly noticeable. The turbulent flow field is rapidly converted into a more intense and organized structure after November-December.

The basic mechanism which controls the flow structure in the surface layer of the northwestern shelf is spreading of the Danube outflow. Wind stress is an additional modifier of the circulation. The Danube anticyclonic eddy confines within a narrow band along the coast between Odessa and Constanta and is introduced by the wind forcing prevailing for almost half of the year during spring and summer months (Fig. 1A.2.5a,b). It sometimes expands and occupies almost the whole NWS region (Fig. 1A.2.5b). The Constanta and Kaliakra anticyclones located further south have a typical lifespan of 50 days and are observed for about 190 days per year.

An alternative configuration of the River Danube plume is the southward coastal current system (Fig. 1A.2.5a). The leading edge of this plume protrudes southward (i.e. downstream) as a thin baroclinic boundary current along the western coastline. The flow system is separated from offshore waters by a well defined front as inferred from the large contrast between the chlorophyll concentrations in the figure. Its offshore flank may display unstable features, exhibits meanders and spawns filaments extending across the wide topographic slope zone (Fig. 1A.2.5b). Except such small scale features, there is almost no exchange between shelf and interior basin.

All available finding of the Black Sea circulation system suggest that the most notable quasi-persistent and/or recurrent features of the circulation system, as schematically presented in Fig. 1A.2.6, include (i) the meandering Rim Current system cyclonically encircling the basin, (ii) two cyclonic sub-basin scale gyres comprising four or more gyres within the interior, (iii) the Bosporus, Sakarya, Sinop, Kizilirmak, Batumi, Sukhumi, Caucasus, Kerch, Crimea, Sevastopol, Danube, Constanta, and Kaliakra anticyclonic eddies on the coastal side of the Rim Current zone, (iv) bifurcation of the Rim Current near the southern tip of the Crimea; one branch flowing southwestward along the topographic slope zone and the other branch deflecting first northwestward into the shelf and then contributing to the southerly inner shelf current system, (v) convergence of these two current systems near the southwestern coast, (vi) presence of a large anticyclonic eddy within the northern part of the northwestern shelf.

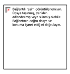

Fig. 1A.2.5. SeaWiFS chlorophyll distributions showing two alternative forms of circulation structure in the northwestern shelf; (a) a southward coastal current system during days 152-155 (early June) and (b) a closed circulation system confined into its northern sector during days 194-197 (mid-July), 1998 (from Oguz et al., 2001).

Lagrangian subsurface current measurements by three autonomous profiling floats deployed into the intermediate layer and deep layers permitted new insights on strength and variability of the flow field (Korotaev et al., 2006). They, for the first time provided direct, quantitative evidence for strong currents and a well organized flow structure that changed the traditional views built on a rather sluggish deep circulation of the Black Sea. The data suggested active role of mesoscale features on the basin-wide circulation system at 200 m similar to the case observed in the upper layer (<100 m) circulation system.? The currents reach a maximum intensity of 15 cm s^{-1} along the Rim Current jet around the basin, which is consistent with the findings of ADCP measurements (Oguz and Besiktepe, 1999).

The magnitudes of deep currents may reach to 5 cm s^{-1} at 1500 m depth along the steep topographic slope (Korotaev et al., 2006). The combination of float and altimeter data suggests that deep currents are steered by the steep topographic slope and well-correlated with the structure of surface currents at seasonal and longer time scales. The deep layer currents flow along the strong topographic slope following constant potential vorticity isoclines due to the topographic β-effect. The wind stress, as the main driving force, can introduce a barotropic flow on the order of 5 cm s^{-1} as further supported by the numerical modeling studies (Stanev, 1990; Oguz et al., 1995; Stanev and Beckers, 1999).? The floats at the intermediate (750 m) and deep (1550 m) layers also delineate the importance of mesoscale eddies on the flow field.

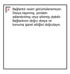

Fig. 1A.2.6 Schematic diagram for major quasi-permanent/recurrent features of the upper layer circulation identified by synthesis of hydrographic studies and analysis of the sea level anomaly altimeter data (modified from Korotaev et al. 2003).

1.2.3. Climatic properties

Water budget: On the basis of available data since the 1920s (Ilyin et al., 2006), the total river discharge and precipitation into the sea show weak but opposite trends that compensate each other and therefore their sum remain uniform at ~550 $km^3 y^{-1}$ (Fig. 1A.2.7). Evaporation varied slightly around 400 $km^3 y^{-1}$ up to the mid 1970s (except 15% increase in the 1940s), and then decreased steadily to ~300 $km^3 y^{-1}$ during the subsequent 15 years and stabilized at this value afterwards. The net fresh water flux into the sea, therefore, revealed an increasing trend from ~120 $km^3 y^{-1}$ in the early 1970s to ~300 $km^3 y^{-1}$ in the mid-1990s with additional fluctuations of ~100 $km^3 y^{-1}$. Its difference from the temporal volume change of the sea (which in fact may be calculated by the sea level data) implies a nearly two-fold change in the net outflow from the Black Sea into the Bosporus during the second half of the 1990s with respect to the 1960s.

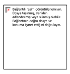

Fig. 1A.2.7 Long-term variations of the river discharge, precipitation, evaporation (km^3 y^{-1}) for the Black Sea together with net water flux and the corresponding net Bosphorus inflow from the Black Sea (after Ilyin et al., 2006).

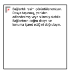

Fig. 1A.2.8. Yearly changes of the Danube discharge (km^3 y^{-1}) during 1960-2005 (data provided by A. Cociasu).

One of the implications of water budget analysis is a continuous trend of decrease of the total river discharge from the early 1980s to the mid-1990s and then an increase during the rest of the 1990s. The Danube discharge was mainly responsible for these changes as it decreased to 100 km^3 y^{-1} in the 1980s (up to 1993) and started increasing again by the same amount during the 1990s (Fig. 1A.2.8). A similar reduction took place once again during 2000-2003, but 2004-2005 was a recovery phase to the level in the 1999. A closer inspection of its monthly variations (Fig. 1A.2.9) in fact reveals two different modes of variations depending on the regional climatic variations. Some years (e.g. 1993, 1995, 2000, 2001, 2002, 2004, and 2005) were characterized only by the spring peak. The years 1994, 1996-1999 attained both winter and spring peaks, whereas no spring discharge occurred in 2003. A limited Danube inflow took place previous autumn and winter months of this particular anomalous year and therefore the Black Sea received the lowest discharge rate from the Danube since the beginning of the 1990s.

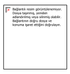

Fig. 1A.2.9. Monthly changes of the Danube discharge (km^3 y^{-1}) during 1993-2005 (blue) and its annual-mean variations (green) (data provided by A. Cociasu).

Sea Surface Temperature: The winter-mean (December-March) sea surface temperature (SST) variations shown in Fig. 1A.2.10 were described by different monthly-mean data sets. The first one was complied by Hadley Centre, UK Meteorological Office from all available in situ measurements within the interior part of the basin with depths greater than 1500 m and Advanced Very High Resolution Radiation (AVHRR) satellite observations (Rayner et al., 2003). The second data set was provided by the Global Ice-Sea Surface Temperature, version 2.2 data set (GISST2.2) for the region confined by 42??44?N latitude range and 29??39?E longitude range during 1950?1994 (Kazmin and Zatsepin, 2007). Other data sets include the NCEP-Reynolds 1^o resolution monthly AVHRR night-time measurements for 1983?2006 and 4 km resolution weekly Pathfinder5 AVHRR night-time measurements for 1987?2005. Fig. 1A.2.10 also shows the minimum Cold Intermediate Layer temperature variation (characterized by temperatures less than 8^{o}C below the seasonal thermocline) as the mean of all available data from the interior basin for May-November period of 1950-1995 (Belokopytov, 1998) and from the regular measurements along several cross-sections within the eastern Black Sea during July-September period of 1990-2004 (Krivosheya et al., 2005).

The winter GISST data reveal an approximately 1.0ºC cooling trend from 9.0ºC in 1970 to 8.0ºC in 1985. The Hadley SST data instead remain uniform at 8.7?0.1ºC during the 1960s and 1970s and then decreased abruptly from about 8.5ºC at 1981 to 7.7ºC at 1984. The cooling phase persists up to 1994 and switches abruptly to the warming mode until 2002 that was then replaced by a cooling mode up to the present. The NCEP-Reynolds data that form a part of the Hadley data set are similar to the Hadley one after 1993. The more recent and refined Pathfinder data set was also similar to the NCEP-Reynolds data after the beginning of the 1990s. The accompanying CIL data support reliability of the Hadley winter SST data because the minimum CIL temperature in summer months reflects signature of the winter SST.? Approximately 0.7ºC difference between the subsurface summer CIL temperature and the winter Hadley SST should probably arise from different spatial averaging of the variable data sets.

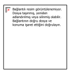

Fig. 1A.2.10. Long-term variations of the basin-averaged winter-mean (December-March) Sea Surface Temperature (SST) during 1960-2005 using the monthly data sets of Hadley Centre-UK Meteorological Office (blue), GISST (Kasmin and Zatsepin, 2007; red), NCEP-Reynolds 1º resolution AVHRR (violet), Pathfinder5 4 km resolution AVHRR (black), minimum temperature of the Cold Intermediate Layer for the mean of May - November period (green), and the winter-mean (December-March) SST measured near Constanta (Romanian coast). All these data were plotted after smoothed by the three point moving average.

Considerable regional variability up to 2ºC between the colder interior basin and warmer peripheral zone irrespective of the interannual variability is a striking feature of the Black Sea (Fig. 1A.2.11). In general, regional meteorological conditions in the eastern part favour milder winters and warmer winter temperatures in the surface mixed layer. Thus the decadal warming signature was felt more pronouncedly in the eastern basin during the 1990s. The western coastal waters receiving the freshwater discharge from Danube, Dniepr and Dniestr Rivers correspond to the coldest parts of the Black Sea that are roughly twice colder than the southeastern corner of the basin irrespective of the year (Fig. 1A.2.11).?

Consistency between the summer-autumn mean CIL temperature and the winter SST variations in terms of both timing and duration of the warm and cold cycles implies propagation of the winter warming/cooling events to 50-60 m depths during rest of the year. The existence of sharp thermocline helps to preserve the CIL signature throughout the year irrespective of the surface mixed layer temperature structure. The high correlation (r=0.89 with significance level=0.99) between the summer-autumn mean CIL temperature and the winter (December-March) mean winter SST allows a rough estimate of the former from the satellite data using the empirical relationship
$T(CIL)=0.619*SST+2.063$.

The summer SST variations differ from the winter ones to a considerable extent (Fig. 1A.2.12; blue). For example, cold winters of 1991-1992 are followed by relatively warm summers with SST ≥ 25ºC in August. Contrary to a steady rise of the winter SST after 1994, summer SSTs remain relatively low (below 24.5ºC) until 1998, and fluctuates between 25ºC and 26ºC afterwards. In-situ measurements along the northeastern coast (Shiganova, 2005) generally support these features (blue line in Fig. 1A.2.12). On the other hand, the annual-mean basin-averaged SST reveals a warming trend from ~14.8ºC in 1989 to 15.6ºC in 2005 with some oscillations along the trend (green line in Fig. 1A.2.12). In particular, 1992, 1993, 1997, 2003 and 2004 emerge as cold years.

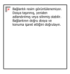

Fig. 1A.2.11. The mean SST distribution in February for 2001 and 2003 obtained from 9 km monthly-mean, gridded NOASS/NASA AVHRR Oceans Pathfinder data set (after Oguz et al., 2003). The curve (in white colour) shows 200 m bathymetry.

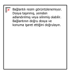

Fig. 1A.2.12. Annual-mean (triangles) and August (dots) SST variations obtained by the basin-averaging of 9 km monthly-mean, gridded NOASS/NASA AVHRR Oceans Pathfinder data, and annual-mean (stars) and August (squares) SST variations measured at Constanta (Romanian coast) and along the northeastern coastal waters (crosses; Shiganova, 2005).

Sea level: It is a prominent feature of global warming as well as large scale atmospheric systems in regional seas.? Sea level change provide best response of the physical climate to atmospheric forcing, because the link includes an overall response of the changes in the surface atmospheric pressure through the inverse barometer effect, water density changes in response to temperature and salinity variations (steric effects), precipitation, evaporation and river runoff.? The detrended sea level anomaly (SLA) time series (Reva 1997, Tsimplis and Josey 2001, Stanev and Peneva 2002), as an average of the measurements at 12 coastal stations around the Black Sea, oscillate within the range of 10 cm (Fig. 1A.2.13a). Its higher (lower) values coincide with the warm (cold) cycles of the water temperature indicating that a part of the observed sea level change has a thermal origin due to the thermo-steric effect. The annual-mean tide-gauge data show a high degree of consistency with the altimeter SLA data as well (Fig. 1A.2.13b). They both exhibit a rising trend of 3 cm y^{-1} from 1993 to the mid-1999 followed by -3.0 cm y^{-1} declining trend for 07/1999?12/2003 in consistent with the cooling phase indicated by the winter SST data. When monthly variations of the SLA are resolved, the linear trend of rise increases to 20 cm during 1992-1999 (Fig.1.2.14) that was roughly 3 cm higher than the estimate based on the coastal tide gauge data (Tsimplis and Josey, 2001; Stanev and Peneva 2002). Good agreement between the monthly SLA changes and the Danube discharge rates suggest its predominant role on the basin-scale sea level oscillations.

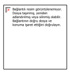

Fig. 1A.2.13a. Long-term variations of the detrended sea level anomaly (blue) after high frequency oscillations have been filtered by the three point moving average and its comparison with annual mean sea level anomaly retrieved from satellite altimeter measurements (after Oguz et al., 2006).

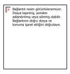

Fig. 1A.2.13b. Comparision of the detrended monthly-mean sea level anomaly obtained from the basin-averaged altimeter data (black) and the mean of 12 coastal sea level stations around the basin (blue)? (after Goryachkin et al., ?2003).

Air Temperature and surface atmospheric pressure: The winter-mean air temperature anomaly data from various coastal stations around the periphery of the basin (Titov, 2000; 2002) exhibit similar temporal variations, even though the mean temperatures and their range of variations may differ from the western to eastern end of the basin. Fig. 1A.2.15 provides an example along the northern coast of the central Black Sea. Fig. 1A.2.15 also includes the spatially averaged 2º resolution data retrieved from the URL site ftp://data.giss.nasa.gov/pub/gistemp/txt/.

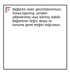

Fig. 1A.2.14. Monthly (blue) and yearly (green) SLA changes in the Black Sea during 1993-2006 together with its long-term trend (brown) and two shorter term trends (yellow) for 1993-1999, 1999-2003, and 2003-2006.

In general, the long-term AT anomaly data since 1885 exhibit a linear warming trend with the overall temperature rise of 0.9 ºC (Oguz et al., 2006). It is consistent with the warming observed in winter temperature over Eurasia that was explained partly by temperature advection from the North Atlantic region (i.e. connected to the NAO) and partly by the radiative forcing due to increased greenhouse gases (Hurrell, 1996).? The last two decades have been subject to its abrupt variations over 10 year cycles (Fig. 1A.2.15). In particular, according to the GISST data set, the winter AT anomaly decreased 2.0ºC during the mid-1970s and 1985-1995. The former was less whereas the latter was more pronounced for the coastal station data. Both the timing and duration of the warm and cold cycles fit reasonably well with the winter-mean (December-March) SST and the summer-autumn (May-November) mean CIL temperature time-series (Fig. 1A.2.10). The agreement between the winter-mean AT anomaly and SST is particularly good for the GISS-based data sets.

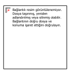

Fig. 1A.2.15. Winter (December-March) mean air temperature anomaly variations measured at the meteorological station near the Kerch Strait (red) and obtained by averaging of the GISST data for the basin (green), and winter (December-March) mean surface atmospheric pressure (hPa) obtained by averaging ERA40 data over the basin (blue).? High frequency oscillations in the data have been filtered by the three point moving average.

The winter (December-March mean) basin-averaged sea level pressure (SLP) distribution over the Black Sea (Fig. 1A.2.15) follows closely the winter air temperature time series.? The severe winters with low air temperatures tend to be associated with higher sea level atmospheric pressures (up to 1021 hPa), whereas lower pressures correspond to milder winter seasons. Decreasing winter air temperature trend during the 1985-1993 is supported by an increasing trend of the winter surface pressure and vice versa for the 1990s.?

Link to teleconnection patterns over the Eurasia: The North Atlantic Oscillation (NAO) defined as an index representing the normalized sea level atmospheric pressure difference between Lisbon, Portugal (for the Azores high pressure system) and Stykkisholmur/Reykjavik, Iceland (for the Icelandic low pressure system) is an important mode of variability of the Northern Hemisphere atmosphere (Marshall et al., 1997). Its positive values for winter (December through March) indicate strong pressure gradient between these two pressure systems that brings cold and dry air masses to southern Europe and Black Sea region by strong westerly winds (Hurrell, et al., 2003). In these periods, the Black Sea region is affected by the Azores high pressure center and thus characterized by the higher surface air pressure values, reduced evaporation and colder air and sea surface temperatures (Fig. 1A.2.16). Conversely, the negative NAO index that implies lower surface atmospheric pressure differences gives rise to milder winters with warmer air temperatures and less dry/more wet atmospheric conditions transported over the Black Sea from the southwest. Various studies in the Mediterranean, Black and Caspian Seas (e.g., Reva, 1997; Ozsoy, 1999; Tsimplis and Josey, 2001; Stanev and Peneva, 2002; Oguz, 2005b; Oguz et al., 2006; Kazmin and Zatsepin, 2007) established a regional dynamical link to the NAO.? The NAO signature has also been recorded in stream flow changes of the Tigris and the Euphrates Rivers (Cullen and deMenocal, 2000), as well as in the River Danube discharge (Polonsky et al., 1997; Rimbu et al., 2004).

The general consistency between periods of positive (negative) NAO index values and relatively low (high) sea surface and air temperatures, higher (lower) surface air pressures supports the presence of a teleconnection between the regional atmospheric conditions and the NAO-driven large scale atmospheric motion (Oguz et al., 2006, Kazmin and Zatsepin, 2007). In terms of duration and intensity of events, the sequence of mild and severe winter cycles follows the temporal pattern of the negative and positive NAO cycles, respectively. In particular, the strong cooling trend during 1980-1993 characterizes an extended strongly positive NAO index phase with an increasing trend. The subsequent warming trend in SST coincides with the weakening of positive NAO index and its decreasing trend.

Krichack et al. (2002) have shown that interannual variability of precipitation over the eastern Mediterranean can be explained more appropriately by the joint analysis of the NAO and EAWR indices which incorporates different possible combinations of a quadrapole system formed by the high and low surface pressure anomaly centers over the North Atlantic and the Eurasia as representative of different states of the eastern Mediterranean atmosphere. Oguz et al. (2006) later adopted this concept for the Black Sea in order to explain some peculiarities of the climatic variations which can not be described well by the NAO alone.

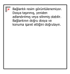

Fig. 1A.2.16. Long-term variations of the winter North Atlantic Oscillation index (blue), East Atlantic-West Russia (EAWR) index (green) and Iceland sea surface temperature (red). High frequency oscillations in the data have been filtered by the five point moving average.

The winter (December-January-February) mean East Atlantic-West Russia (EAWR) index represents the zonal shift between quasi-persistent high and low surface pressure anomaly centers over the Western Europe and the Caspian region (Fig. 1A.2.16). This system characterizes the second strongest mode of the North Atlantic climate (Molinero et al., 2005) and zonally modulates the NAO over the Eurasia continent. Its positive phase (EAWR index > 0) results from the joint effect of the increased anticyclonic anomaly center over the North Sea and the increased cyclonic anomaly center over the Caspian Sea. The Black Sea region is then exposed to cold and dry air masses from the northeast-to-northwest sector. Alternatively, its negative phase (EAWR index < 0) is associated with the cyclonic anomaly center over the North Sea and the anticyclonic activity over the Caspian Sea (i.e. relatively low pressure difference over the Europe). In this case, the Black Sea region is affected by warmer and wetter winter conditions under the influence of increased southwesterlies-to-southeasterlies. They resemble closely the North Sea-Caspian Pattern (NCP) index introduced using 500 hPa geopotential anomaly patterns by Kutiel and Benaroch (2002).

When both NAO>0 and EAWR>0, the system was governed by the low pressure anomaly centers over Iceland and Caspian Sea and a high pressure anomaly centers over Azores and the North Sea. This case leads to strongest cold winters in the Black Sea due to cold air mass outbreaks from the northwest and/or the northeast as in the case of early 1990s.? When NAO>0 and EAWR<0, the Caspian low is replaced by an anticyclonic anomaly center, and the Black Sea region is then controlled by either cold air outbreaks from the northwest or warm air outbreaks from the southeast depending on the relative strengths and spatial coverages of the Icelandic low and Caspian high pressure systems. This case applies to the period of 1970-1975 and may be the reason for a weak cooling signature noted in the SST even if the NAO was in strong positive mode. The reverse case of NAO<0 and EAWR>0 gives rise to the cold winters with cold air outbreaks from the northern sector. Alternatively, the warm and mild winters may also prevail when the Azores high pressure system is sufficiently strong and protrudes towards the east.? As suggested by the Black Sea hydro-meteorological time series data, the latter case occurred during the 1960s and 1990s. When both NAO<0 and EAWR<0, the system is affected by the warm air mass intrusions from the southwest-southeast sector giving rise to mild winters in the Black Sea. Its typical example was observed during the second half of the 1970s.

The decadal variations observed in the Black Sea hydro-meteorological properties are consistent to some extent solar (sun spot) variations having the 10-12 year periodicity.? The periods of solar minima coincide with reduced air and sea surface temperatures, which generally correspond to the periods of positive NAO index values. In contrast, the periods of solar maxima coincide with the periods of higher air and sea surface temperatures characterized by negative values in the NAO index. A positive correlation exists between the SST and the sunspot number for each five year bins of the consecutive cold and warm cycles of the 1960-2000 phase. The in-phase variations between the sun spot number and the regional hydro-meteorological characteristics may suggest possible impact of the solar activity its link to the lower atmosphere and subsequently air and sea surface temperatures of the Black Sea.

References

Afanasyev, Y.D., Kostianoy, A.G., Zatsepin, A.G., and Poulain P.M. (2002) Analysis of velocity field in the eastern Black Sea from satellite data during the Black Sea ?99 experiment. J. Geophys. Res., 107, 10.1029/2000JC000578.

Beckers, J.M., Gregoire, M.L., Nihoul, J.C.J., Stanev, E., Staneva, J. and Lancelot C. (2002) Hydrodynamical processes governing exchanges between the Danube, the north-western continental shelf and the Black Sea's basin simulated by 3D and box models. Estuarine, Coastal and Shelf Science, 54, 453-472.

Belokopytov, V. (1998) Long-term variability of Cold Intermediate Layer reneval conditions in the Black Sea. In Ecosystem modeling as a management tool for the Black Sea, NATO Sci. Partnership Sub-ser., 2, vol. 47, edited by Ivanov, L? and Oguz, T., Vol 2, 47-52 pp, Kluwer Academic Publishers.

Besiktepe, S.T., Lozano, C.J., and Robinson A.R. (2001) On the summer mesoscale variability of the Black Sea. J. Mar. Res., 59, 475-515.

Buesseler, K.O., Livingston, H.D., Ivanov, L. and Romanov, A. (1994) Stability of the oxic-anoxic interface in the Black Sea. Deep-Sea Res. I, 41, 283-296.

Cullen, H.M., and de Menocal, P.B. (2000) North Atlantic Influence on Tigris-Euprates streamflow. Int. J. Climatol., 20, 853-863.

Faschuk, D.Ya., Ayzatullin, T.A., Dronov, V.V, Pankratova, T.M. and Finkelshteyn, M.S. (1990) Hydrochemical structure of the layer of co-existence of oxygen and hydrogen sulfide in the Black Sea and a possible mechanism of its generation. Oceanology (English transl.), 30, 185-192.

Gawarkiewicz, G., Korotaev, G. Stanichny, S., Repetin, L. and Soloviev, D. (1999) Synoptic upwelling and cross-shelf transport processes along the Crimean coast of the Black Sea. Cont. Shelf Res., 19, 977-1005.

Ginsburg, A.I., Kostianoy, A.G., Soloviev, D.M., Stanichny, S.V. (2000) Remotely sensed coastal/deep-basin water exchange processes in the Black Sea surface layer. In Satellites, Oceanography and Society, D. Halperneds. Elsevier Oceanography Series, Amsterdam, 63, pp. 273-285.

Ginsburg, A.I., Kostianoy, A.G., Nezlin, N.P., Soloviev, D.M., Stanichny, S.V. (2002a) Anticyclonic eddies in the northwestern Black Sea. J. Mar. Syst., 32, 91-106.

Ginsburg, A.I., Kostianoy, A.G., Krivosheya, V.G., Nezlin. N.P., Soloviev, D.M, Stanichny, S.V., Yakubenko, V.G. (2002b) Mesoscale eddies and related processes in the northeastern Black Sea. J. Mar. Syst., 32, 71-90.

Glazer, B.T., Luther III, G.W. Konovalov, S. K., Friederich, G. E., Trouwborst, R.E., Romanov, A.S. (2006) Spatial and temporal variability of the Black Sea suboxic zone. Deep Sea Res. II, 53,1756-1768.

Gregg, M. C. and Yakushev, E. V. (2005) Surface Ventilation of the Black Sea?s Cold Intermediate Layer in the Middle of the Western Gyre. Geophys. Res. Lett. 32, L03604.

Goryachkin, Yu. N., Ivanov, V. A., Lemeshko, E. M., and Lipchenko, M. M. (2003) Application of the altimetry data to the analysis of water balance of the Black Sea. Physical Oceanography, 13, 355-360.

Hiscock, W.T. and Millero, F. J. (2006) Alkalinity of the anoxic waters in the Western Black Sea. Deep Sea Res. II, 53,1787-1801.

Hurrell, J.W. (1996) Influence of variations in extratropical wintertime teleconnections on Northern Hemisphere temperature. Geophys. Res. Lett., 23, 665-668.

Hurrell, J.W., Kushnir, Y., Ottersen, G., and Visbeck, M. (2003) An overview of the North Atlantic Oscillation. In The North Atlantic Oscillation: Climatic Significance and Environmental Impact, Geophysical Monograph 134, Edited by J.W. Hurrell, Y. Kushnir, G. Ottersen, M. Visbeck, 1-36pp, published by American Geophysical Union, Washington DC.

Ilyin, Y.P. and Repetin, L.N. (2005) Long-term climatic trends in the Black Sea region and their seasonal features. Proceedings of The First

Biannual Scientific Conference: Black Sea Ecosystem 2005 and Beyond, organized by Commission on the Protection of the Black Sea Against Pollution, May 2006, Istanbul.

Ivanov, L.I. and Samodurov, A.S. (2001) The role of lateral fluxes in ventilation of the Black Sea. J. Mar. Syst., 31, 159-174.

Jannasch, H.W., Wirsen, C.O. and Molyneaux, S.J. (1991) Chemoautotrophic sulfur-oxiding bacteria from the Black Sea. Deep-Sea Res., 38, Suppl.2A, S1105-S1120.

Jorgensen, B.B., Fossing, H., Wirsen, C.O. and Jannasch, H.W. (1991) Sulfide oxidation in the anoxic Black Sea chemocline. Deep-Sea Res., 38, Suppl.2A, S1083-S1104.

Karl, D.M., and Knauer, G.A. (1991) Microbial production and particle flux in the upper 350 m of the Black Sea. Deep Sea Res., 38, Supp. 2A, S655-S661.

Kazmin, A.S. and Zatsepin, A.G. (2007) Long-term variability of surface temperature in the Black Sea, and its connection with the large-scale atmospheric forcing. J. Mar. Syst., 68, 293?301.

Konovalov, S.K., and Murray, J.W. (2001) Variations in the chemistry of the Black Sea on a time scale of decades (1960-1995). J. Mar. Syst., 31, 217-243.

Korotaev, G.K., Saenko, O.A., Koblinsky, C.J. (2001) Satellite altimetry observations of the Black Sea level. J. Geophys. Res., 106, 917-933.

Korotaev, G.K., Oguz, T., Nikiforov, A., Koblinsky, C. J. (2003) Seasonal, interannual and mesoscale variability of the Black Sea upper layer circulation derived from altimeter data. J. Geophys. Res., in press.

Korotaev, G., Oguz, T., Riser, S. (2006) Intermediate and deep currents of the Black Sea obtained from autonomous profiling floats. Deep Sea Res. II, 53, 1901-1910.

Krivosheya, V.G., Titov, V. B., Ovchinnikov, I.M., Kosyan, R.D., Skirta A.Yu. (2000) The influence of circulation and eddies on the depth of the upper boundary of the hydrogen sulfide zone and ventilation of aerobic waters in the Black Sea. Oceanology (Eng. Transl.), 40, 767-776.

Kuypers, M.M.M., Sliekers, A.O., Lavik, G., Schmid, M., Jorgensen, B.B., Kuenen J.G., Sinninghe, D.J.S., Strous, M. and Jetten, M.S.M. (2003) Anaerobic ammonium oxidation by anammox bacteria in the Black Sea. Nature, 422, 608-611.

Lebedeva, L.P. and Vostokov, S. V. (1984) Studies of detritus formation processes in the Black Sea. Oceanology (Engl. Transl.), 24(2), 258-263.

Lee, B-S., Bullister, J.L., Murray, J.W. and Sonnrup, R.E. (2002) Anthropogenic chlorofluorocarbons in the Black Sea and the Sea of Marmara. Deep-Sea Res. I, 49, 895-913.

Marshall, J., Kushnir, Y., Battisti, D., Chang, P., Hurrell, J., McCartney M., and Visbeck, M. (1997) A North Atlantic Climate Variability: phenomena, impacts and mechanisms.Inter. Jour. Climatology, 21(15), 1863-1898.

Molinero, J. C., Ibanez, F., Nival, P., Buecher, E. and Sousssi, S. (2005) North Atlantic climate and northwestern Mediterranean plankton variability.? Limnol. Oceanogr., 50(4), 1213-1220.

Murray, J.W., Jannash, H. W., Honjo, S., Anderson, R. F., Reeburgh W.S., Top, Z., Friederich, G.E., Codispoti, L.A. and Izdar, E. (1989) Unexpected changes in the oxic/anoxic interface in the Black Sea. Nature, 338, 411-413.

Murray, J. W., Top, Z. and Ozsoy, E. (1991) Hydrographic properties and ventilation of the Black Sea. Deep-Sea Res., 38, Suppl.2A, S663-690.

Oguz, T. (2005) Black Sea ecosystem response to climate teleconnections. Oceanography, 18(2), 118-128.

Oguz, T. and Ediger, D. (2006) Comparision of in situ and satellite-derived chlorophyll pigment concentrations, and impact of phytoplankton bloom on the suboxic layer structure in the western Black Sea during May?June 2001. Deep Sea Res. II, 53, 1923-1933.

Oguz, T., La Violette, P., Unluata, U. (1992) Upper layer circulation of the southern Black Sea: Its variability as inferred from hydrographic and satellite observations. J. Geophys. Res., 97, 12569-12584.

Oguz, T., Aubrey, D.G., Latun, V.S., Demirov, E., Koveshnikov, L., Sur, H.I., Diacanu, V., Besiktepe, S., Duman, M., Limeburner, R., and Eremeev, V.V. (1994) Mesoscale circulation and thermohaline structure of the Black sea observed during HydroBlack'91. Deep Sea Research I, 41, 603-628.

Oguz, T., Malanotte-Rizzoli, P., and Aubrey, D. (1995) Wind and thermohaline circulation of the Black Sea driven by yearly mean climatological forcing. J. Geophys. Res., 100, 6846-6865.

Oguz. T, Ivanov, L.I., and Besiktepe, S. (1998) Circulation and hydrographic characteristics of the Black Sea during July 1992. In: Ecosystem

Modeling as a Management Tool for the Black Sea, L. Ivanov and T. Oguz (eds). NATO ASI Series, Environmental Security-Vol.47, Kluwer Academic Publishers, Vol. 2, pp.69-92.

Oguz, T., Deshpande, A. G. and Malanotte-Rizzoli, P. (2002a) On the role of mesoscale processes controlling biological variability in the Black Sea: Inferrences from SeaWIFS-derived surface chlorophyll field. Continental Shelf Research, 22, 1477-1492.

Oguz, T., Cokacar, T., Malanotte-Rizzoli, P. and Ducklow, H. W. (2003) Climatic warming and accopanying changes in the ecological regime of the Black Sea during 1990s. Global Biogeochem. Cycles, 17(3), 1088,doi:10.1029/2003.

Oguz T., Dippner, J.W. and Kaymaz, Z. (2006) Climatic regulation of the Black Sea hydro-meteorological and ecological properties at interannual-to-decadal time scales. J. Mar. Syst., 60, 235-254.

Ozsoy, E. and Unluata, U. (1997) Oceanography of the Black Sea: A review of some recent results. Earth Sci. Rev., 42, 231-272.

Ozsoy, E. (1999) Sensitivity to global change in temperate Euro-Asian Seas (The Mediterranean, Black Sea and Caspian Sea): A review. In The Eastern Mediterranean as a laboratory basin for the assessment of contrasting ecosystems, NATO Sci. Partnership Sub-ser., 2, vol. 51, edited by Malanotte-Rizzoli, P., and Eremeev V., 281-300 pp, Kluwer Academic Publishers.

Polat, S.?. and Tugrul, S. (1995) Nutrient and organic carbon exchanges between the Black and Marmara Seas through the Bosphorus Strait. Continental Shelf Research, 15, 1115-1132.

Polonsky, A. B, Basharin, D.V. Voskresenskaya, E.N. and Worley, S. (2004) North Atlantic Oscillation: description, mechanisms, and influence on the Eurasian climate. Phys. Oceanogr., 15(2), 96-113.

Pierre-Marie P., Barbanti, R. Motyzhev, S. and Zatsepin A. (2005) Statistical description of the Black Sea near-surface circulation using drifters in 1999?2003. Deep-Sea Res. I, 52, 2250?2274.

Repeta, D.J. and Simpson, D.J. (1991) The distribution and recycling of chlorophyll, bacteriochlorophyll and carotenoids in the Black Sea. Deep-Sea Res., 38, Suppl.2A, S969-S984.

Repeta, D.J., Simpson, D.J. Jorgensen, B.B. and Jannash, H.W. (1989) Evidence for anoxic photosynthesis from distribution of bacteriochlorophylls in the Black Sea. Nature, 342, 69-72.

Reva, Yu.A. (1997)? Interannual oscillations of the Black Sea level. Oceanology (Eng. Transl.), 37, 193-200.

Rimbu, N., Dima, M. Lohmann, G. and Stefan, S. (2004) Impacts of the North Atlantic oscillation and the El Nino-southern oscillation on Danube river frlo variability. Geophs. Res. Lett., 31, L23203, doi:10.1029/2004GL020559.

Rozanov, A.G., Neretin, L.N. and Volkov, I.I. (1998) Redox Nepheloid Layer (RNL) of the Black Sea: Its location, composition and origin. In: Ecosystem Modeling as a Management Tool for the Black Sea. L. Ivanov and T. Oguz, eds. NATO ASI Series, 2-Environmental Security-47, Kluwer Academic Publishers, Vol. 1, pp.77-92.

Shiganova, T. (2005) Gelatinous plankton surveys in the Ponto-Caspian Seas. Proceedings of The First Biannual Scientific Conference: Black Sea Ecosystem 2005 and Beyond, organized by Commission on the Protection of the Black Sea Against Pollution, May 2006, Istanbul.

Sokolova, E., Stanev, E.V., Yakubenko, V., Ovchinnikov, I. and Kosyan, R. (2001) Synoptic variability in the Black Sea. Analysis of hydrographic survey and altimeter data. J. Mar. Syst., 31, 45-63.

Sorokin, Y.I. (1972) The bacterial population and the process of hydrogen sulfide oxidation in the Black Sea. J. Conseil Int. pour l'Explorotion de la Mer, 34, 423-454.

Stanev, E.V. (1990) On the mechanisms of the Black sea circulation. Earth-Sci. Rev., 28, 285?319.

Stanev, E. V. and Beckers, J.M. (1999) Numerical simulations of seasonal and interannual variability of the Black Sea thermohaline circulation. J. Mar. Syst., 22, 241-267.

Stanev, E.V. and Peneva, E. (2002) Regional sea level response to global climatic change: Black Sea examples. Global and Planetary Changes, 32, 33.47.

Staneva, J.V., Dietrich, D.E., Stanev, E.V. and Bowman, M.J. (2001) Rim Current and coastal eddy mechanisms in an eddy-resolving Black Sea general curculation model. J. Mar. Systs., 31, 137-157.

Sur, H.I. and Ilyin, Y.P. (1997) Evolution of satellite derived mesoscale thermal patterns in the Black Sea. Prog. Oceanogr., 39, 109-151.

Sur, H.I., Ozsoy, E. and Unluata, U. (1994) Boundary current instabilities, upwelling, shelf mixing and eutrophication processes in the Black Sea. Progr. Oceanogr., 33, 249-302.

Sur, H.I., Ozsoy, E. Ilyin, Y.P., Unluata, U. (1996) Coastal/deep ocean interactions in the Black Sea and their ecological/environmental impacts. J. Marine Systems, 7, 293-320, 1996.

Titov, V.B. (2000) Dependence of the formation of the winter hydrological structure in the Black Sea on the severity of winter conditions. Oceanology (Engl. Transl.), 40, 777-783.

Titov, V.B. (2002) Seasonal and interannual variability of climatic conditions over the Black Sea, in the Black Sea, in Multidisciplinary investigations of the northeast part of the Black Sea, edited by A.G. Zatsepin and M.V. Flint, pp.9-19, Moscow, Nauka.

Trouwborst, R. E., Clement, B. G., Tebo, B. M., Glazer, B. T., Luther III, G. W. (2006) Soluble Mn(III) in suboxic zones. Science, 313, 1955-1957.

Tsimplis, M.N. and Josey, S.A. (2001) Forcing of the Mediterranean Sea by atmospheric oscillations over the North Atlantic. Geophys. Res. Lett., 28, 803-806.

Tugrul, S., Basturk, O. Saydam, C. and Yilmaz, A. (1992) The use of water density values as a label of chemical depth in the Black Sea. Nature, 359, 137-139.

Zatsepin, A.G., Ginzburg, A.I., Kostianoy, A.G., Kremenitskiy, V.V., Krivosheya, V.G., Stanichny, S.V., and Poulain, P-M. (2003) Observations of Black Sea mesoscale eddies and associated horizontal mixing. J. Geophys. Res., 108, 3246, doi:10.19/2002JC001390.

Zatsepin A. G. , Golenko, N. N., Korzh, A. O., Kremenetskii, V. V., Paka, V. T., Poyarkov, S. G., and Stunzhas, P. A. (2007) Influence of the dynamics of currents on the hydrophysical structure of the waters and the vertical exchange in the active layer of the Black Sea. Oceanology, 47(3), 301?312.

Related

State of Environment of the Black Sea (2002) Implementation of the Black Sea Strategic Action Plan Report (2002) Implementation of the Black Sea Strategic Action Plan Report (2009)

Download part 1, part 2

Publications

Newsletter No 14

Phytoplankton Manual

Black Sea Non-Native Fish List

Black Sea Fishes List IUCN Status

Guidelines for Quality Control of Biological Data - Phytoplankto ...

Kecrch Report

Newsletter No 13

Final Diagnostic Report to guide improvements to the regular rep ...

Black Sea Fishes Check List

Is the number of jellyfish increasing as the Black Sea is warmin ...

Newsletter No 12

State of the Environment of the Black Sea (2002/2007)

Implementation of the Black Sea Strategic Action Plan (2002/2007 ...

Newsletter No 11

Marine Litter Report

2nd Black Sea Scientific Conference Proceedings

1st Black Sea Scientific Conference Proceedings

Newsletter No 10

[Manual for Quantitative Sampling and Sample Treatment of Marine ...]

[Good Practices in Project Preparation]

[Newsletter No 9]

[Newsletter No 8]

[Newsletter No 7]

[Implementation of the Black Sea Strategic Action Plan 1996 - 200 ...]

[State of Environment of the Black Sea 1996 - 2000]

Filter

- Show text only
- Show figures only
- Show tables only
- **Show all**

Font Size

10 12 14 16 18 20 22 24

reset

Highlight Text

Highlighting tool coming soon

Quick Search Tool

enable quick search

Search SOE 2009 whole site

Search >>

Select a text or type in the search box above ...